Dynamic light scattering and angular dissymmetry for the *in situ* measurement of silicon dioxide particle synthesis in flames

Michael R. Zachariah, D. Chin, H. G. Semerjian, and J. L. Katz

Particle size measurements have been made of silica formation in a counterflow diffusion flame reactor utilizing dynamic light scattering and angular dissymmetry methods. The results suggest that the techniques compare quite favorably in conditions of high signal to noise. However, the dynamic light scattering technique degrades rapidly as the signal strength declines, resulting in erroneously small particle diameters. As a general rule dynamic light scattering does not seem to possess the versatility and robustness of the classical techniques as a possible on-line diagnostic for process control. The drawbacks and limitations of the two techniques are also discussed.

I. Introduction

Current interest in exploiting ceramics for their unique structural, optical, and electrical properties has focused attention on the synthesis techniques which may be employed. One area of interest to the ceramist is the production of submicron particles of known size, polydispersity, and shape. This necessarily requires an appreciation of the synthesis environment as well as appropriate diagnostic techniques for particle characterization.

The reacting medium provided by flames is one of the environments utilized for synthesis of ceramics. Indeed, a number of products including fumed silica (SiO_2) and titanium dioxide (TiO_2) are produced industrially via a combustion environment.[1] A large variety of diagnostic techniques have been utilized in the past to characterize particle formation in flow systems; most of these are optical techniques which provide *in situ* nonintrusive measurements with high temporal and spatial resolution. As a rule, these techniques rely on light scattering from particles, although there are a number of variations on the basic concept, including scattering-to-extinction ratio, two-color measurements, polarization ratio, and angular dissymmetry.[2,3] All the above-mentioned techniques fall into the class of what is generally referred to as ensemble elastic light scattering (ELS) methods. Along a different line are the dynamic light scattering (DLS) methods (quasielastic), which are a relatively new development in particle measurement.[4]

There have been few *in situ* comparisons between DLS and ELS methods. King *et al.*[5] in comparing the results between DLS and scattering/extinction on small soot particulates (<20 nm) found DLS measured diameters to be in some cases more than a factor of 3 smaller. By comparison, Flower's[6] measurements on soot yielded particle diameters within 10% for the two techniques. This paper will discuss the results of measurements obtained from DLS and angular dissymmetry for the *in situ* characterization of fumed silica particle formation in counterflow diffusion flames, as well as highlight the relative virtues and drawbacks of the techniques as they pertain to their use as an on-line diagnostic.

II. Dynamic Light Scattering

Dynamic light scattering, also known as photon correlation spectroscopy, has found increased use as a means of noninvasive particle sizing particularly in the measurement of soot formation.[7,8] Particles in a probe volume which has been illuminated with monochromatic light will give rise to fluctuations in the scattering field resulting from the Brownian motion of particles. These fluctuations may be envisioned as arising due to a moving diffraction grating (particles), from which scattered light undergoes interference. One can correlate these fluctuations to the mean speed or alternatively the particle diffusion coefficient, which may in turn be related, under appropriate assumptions to be discussed, to a particle diameter. As

J. L. Katz is with Johns Hopkins University, Department of Chemical Engineering, Baltimore, Maryland 21212; the other authors are with U.S. National Institute of Standards & Technology, Center for Chemical Engineering, Gaithersburg, Maryland 20899.

Received 6 June 1988.

there have been extensive theoretical discussions pertaining to DLS in the literature,[4,9-11] this paper highlights only those points important in understanding and implementing the technique.

The fluctuating interference pattern, when imaged on a photomultiplier, produces a corresponding fluctuating photocurrent (homodyne), which may be processed directly by correlation methods[9] or low pass filtered to remove sum frequencies and subsequently Fourier transformed to the frequency domain spectrum centered at 0 Hz. As both approaches yield the same result, the choice is based on the equipment available. Having processed our signal through the frequency domain route, the discussion will follow along those lines. The low pass filtering and subsequent transform processes may be performed through appropriate software, or more conveniently, the task may be performed via a spectrum analyzer.

For monodisperse spherical particles undergoing no mean motion, the resulting power spectra in frequency space takes the form of a Lorentzian[11]:

$$P(\omega) = \frac{2I^2K^2D/\pi}{(2K^2D)^2 + \omega^2} + \text{shot noise} \tag{1}$$

centered at 0 Hz; I is the intensity of scattered light, D is the particle diffusion coefficient, and K is the magnitude of the scattered wave vector as defined by

$$K = \frac{4\pi}{\lambda_0} \sin \theta/2, \tag{2}$$

where λ_0 is the wavelength of the illuminating source and θ is the scattering angle measured relative to the forward scattering direction.

An experimentally measured diffusion coefficient for the particles may be extracted from Eq. (1) by noting the direct proportionality between the frequency at half-maximum (HW = halfwidth at half-max) and the diffusion coefficient

$$HW = \frac{DK^2}{\pi} \text{ Hz}. \tag{3}$$

Clearly an understanding of the nature of particle transport processes is necessary to make reasonable inferences about particle size from the measured power spectra. The underlying transport processes are relatively well established, yet still represent an area of active research, especially with regard to irregularly shaped particles.[12] For the purposes of this discussion, particles are considered to be spherical.

The particle diffusion coefficient in turn may be used in conjunction with the Stokes-Einstein expression[4] to calculate a particle diameter from the functional dependence of particle size on the friction coefficient

$$D = \frac{kT}{f}. \tag{4}$$

For particles in the continuum regime ($l/d \ll 1$), the friction coefficient f for particle drag takes on the familiar form of Stokes law:

$$f = 3\pi\eta d, \tag{5}$$

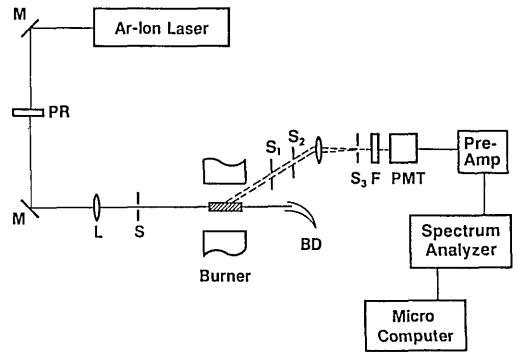

Fig. 1. Schematic representation of the dynamic light scattering system: M, mirror; PR, polarization rotator; L, lens; BD, beam dump; S_1,S_2,S_3, spatial filters; f, narrowband filter; PMT, photomultiplier.

where η is the gas viscosity, and d is the particle diameter.

If the particles are in the free molecular regime ($l/d \gg 1$), the drag on a particle is less than that predicted by Stokes law, and expressions derived from kinetic theory become more appropriate under these conditions[13]:

$$f = \frac{2d^2\rho}{3}\left\{\frac{2\pi kT}{M}\right\}^{1/2}\left\{1 + \frac{\pi\alpha}{8}\right\}, \tag{6}$$

where ρ is the gas density, M is the molecular weight, and α is the accommodation coefficient ($\alpha \approx 0.9$). It should be noted that in going from a particle in continuum to one in free molecular flow, the friction coefficients' dependence on particle diameter changes from d to d^2. To account for continuum free molecular and transition regimes, an empirical interpolation formula is commonly employed[13]:

$$f = \frac{3\pi\eta d}{C}, \tag{7}$$

where C is a slip correction factor.

$$C = 1 + \frac{2l}{d}\left(A_1 + A_2 \exp\frac{-A_3 d}{l}\right), \tag{8}$$

and A_1, A_2, and A_3 are experimentally determined constants[14] ($A_1 = 1.257$, $A_2 = 0.400$, $A_3 = 0.55$). It should be noted that determination of a particle diameter from the measured diffusion coefficient requires knowledge of the local temperature to evaluate the local viscosity, density, and meanfree path needed in the above expressions. Furthermore, some knowledge of the gas composition is necessary to evaluate the above coefficients.

An illustration of the dynamic light scattering system is shown in Fig. 1. The illuminating source is a 4-W argon-ion laser operating at 514.5 nm with an incident power of 1.5 W. A polarization rotator is used to provide perpendicular polarization relative to the measurement plane. The laser is weakly focused into the scattering volume with a 500-mm lens, providing a beam waist of ~0.2 mm. Scattered light is collected at shallow angles ranging from 6 to 10° from the forward scattering angle; spatial filters are used to define the

probe volume. The scattered light is then focused with a 10-cm focal length lens on to a photomultiplier after having passed through a polarizer and laser line filter for the 514.5-nm line ($\Delta\lambda = 1$ nm). The use of a polarizer on the scattered light eliminates the possibility of cross-polarization effects due to scattering from nonspherical particles undergoing rotational motion.

The nature of DLS imposes an additional constraint on the detection optics resulting from the requirement of spatial coherence in the scattered light imaged on the detector. Spatial coherence refers to that region of space from which scattered light from randomly spaced particles will interfere due to their relative phase differences. If the particles are allowed to move about, so will the interference pattern, which, if imaged on a detector, results in a fluctuating photocurrent corresponding to the fluctuating interference pattern. If the detector area is larger than the coherence area, the fluctuating component of the photocurrent will be correspondingly decreased. The DLS signal-to-noise ratio is directly proportional to the ratio of the coherence-to-detector area. In the limit of a large relative detector area, the resulting signal is simply the classical dc light scattering signal. The coherence area for a cylindrical scattering volume of diameter a and length L is given by

$$A_{\text{coh}} = \frac{2R^2\lambda^2}{a(L\sin\theta + a|\cos\theta|)}, \tag{9}$$

where R is the distance from the scattering volume to aperture S_2, L (1.2 cm) and a (0.2 mm) are the length and diameter, respectively, of the scattering volume. The objective is to make the coherence area as large as possible relative to the detector area (area of aperture S_2) by decreasing either the scattering volume or the detector area while still maintaining a detectable signal. Clearly these two factors work in opposition, and, unless one is photon counting, it may be necessary to sacrifice a small detector area to see any signal. As a consequence of the above limitations on signal intensity the ratio of detector area to A_{coh} for our experiments was of the order of 10.

It should be noted that a Lorentzian line shape is only applicable when particles possess no mean motion (either from convected fluid flow or force fields). When mean particle motion is significant, the Lorentzian profile is modified by a Doppler component (Gaussian) to form a Voigt profile.[11] The criteria for selecting the appropriate fitting profile are based on an analysis of two characteristic times, τ_d (diffusion time) and τ_v (transit time through laser beam):

$$\tau_d = 1/(2K^2D), \tag{10}$$

$$\tau_v = a/V, \tag{11}$$

where V is the mean particle velocity.

In conditions where the particle mean motion dominates ($\tau_v \ll \tau_d$), the spectrum will be Gaussian and provide information on particle velocity. If these characteristic times are of the same order a Voigt profile is needed and information on both particle velocity and size can be extracted. Finally, if $\tau_v \gg \tau_d$, particles may be assumed to possess no mean velocity and a Lorentzian is the appropriate form of the spectrum. As a general rule a Lorentzian may always be used in conditions where $\tau_d < 0.25\tau_v$. Calculations made in the present experimental conditions yielded a transit time of ~2 ms and a diffusion time of ~0.02 ms, validating use of a Lorentzian fit.

III. Light Scattering Dissymmetry (LSD)

Angular dissymmetry is one of several light scattering techniques currently used for particle characterization. The scattering-to-extinction ratio technique most commonly used in soot particle measurements is not applicable to the study of silica particles which only possess a real component to the refractive index ($n = 1.46$). Polarization ratio measurements tend not to be a useful tool for measurements on agglomerated particles due to depolarization effects resulting from nonspherical scatterers. Finally, two-color techniques are generally more costly to implement and provide only a small dynamic range. The dissymmetry technique relies on measuring the angular dependence of scattered radiation to infer a particle size. The method requires one to know the refractive index of the scatterer, which may be a limitation on the technique in circumstances where the optical properties of the scatterer are not well established.

To observe any angular dependence in the scattered light, the size of the particle must be larger than the Rayleigh limit as defined by the Mie parameter X ($X = \pi d/\lambda \approx 0.3$). This limit defines the smallest particle which may be sized by dissymmetry for any given wavelength of light. Finally, since in general no *a priori* knowledge of the shape is available, the general assumption is that the particles are spherical.

In its general form, the scattering intensity will be governed by the following relation:

$$Q_{vv}(X,\theta) = C_{vv}(X,\theta)NSR(\theta), \tag{12}$$

where $C_{vv}(x,\theta)$ is the Mie scattering cross section for monodisperse spheres and the subscripts refer to the state of polarization of the incident and detected scattered light (v = vertical). N is the total number of scatterers in the probe volume and SR is the system response function of the optical and electronics system which may be obtained by calibration against a molecule of known scattering cross section (ethene). By obtaining the dissymmetry ratio R_{ij} one eliminates the dependence on number density and may explicitly determine a scattering diameter from a Mie theory calculation[15]:

$$R_{ij} = \frac{C_{vv}(X,\theta i)}{C_{vv}(X,\theta_j)}, \tag{13}$$

Once a particle diameter is determined, the scattering intensity and corresponding scattering cross section for any one of the scattering angles may be used in Eq. (12) to obtain the number density. This number density in turn may be related to a particle volume fraction ϕ:

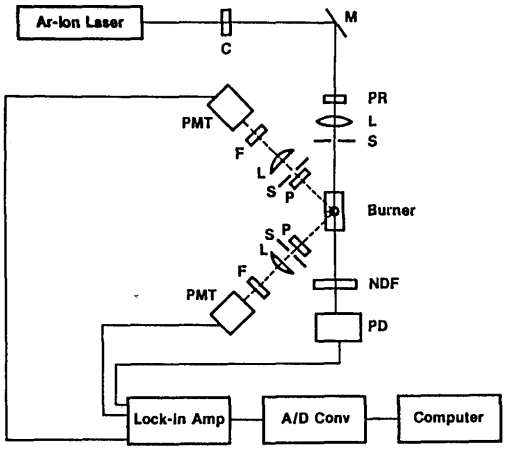

Fig. 2. Schematic representation of scattering dissymmetry measurement system: *C*, chopper; *M*, mirror; *PR*, polarization rotator; *L*, lens; *S*, spatial filter; *P*, polarizer; *F*, narrowband filter; *PMT*, photomultiplier; *NDP*, neutral density filter; *PD*, photodiode.

$$\phi = \frac{\pi}{6} N d^3. \tag{14}$$

A schematic of the light scattering system is illustrated in Fig. 2. It consists of a 4-W argon-ion laser operating on the 514.5-nm line. Incident laser power was set at 0.5 W and modulated with a mechanical chopper at 1018 Hz. A polarization rotator is used to orient the direction of polarization perpendicular to the measurement plane. The beam was focused using the same optical arrangement used in the DLS experiment with scattered light detected at 45 and 135° relative to the forward scattering direction. The detection optics at each angle consisted of a polarizer to reject cross-polarization effects, a collection lens, and a pinhole aperture which defined the length of the sample volume to be 1 mm. In addition, to confine the detector response to light scattered from the particles, a laser line filter centered at $\lambda = 514.5$ nm ($\Delta\lambda = 1$ nm) was employed. The detection electronics consisted of three lock-in amplifiers, one each for the two scattering angles and the third for the extinction leg. The outputs from the lock-ins were digitized at 10 Hz for 10 s (100 data points) and subsequently sent to a microcomputer.

IV. Silica Synthesis Flame Reactor

The choice of reactor has a great influence on the final product, the ease of study, and the eventual information which may be extracted from appropriately chosen experiments. The reactor geometry used here is a counterflow diffusion burner as illustrated in Fig. 3. The advantage of this geometry is that, along the stagnation point streamline (dark solid line in Fig. 3), the flow may be described as a 1-D flow, which greatly reduces the number of measurements required. The reactor consists of two vertically mounted brass counterflowing rectangular ducts separated by a distance of 15 mm. The flow is constrained in two dimensions (x–y plane) with fused silica windows placed on the sides of the smaller cross-sectional dimension. A more ex-

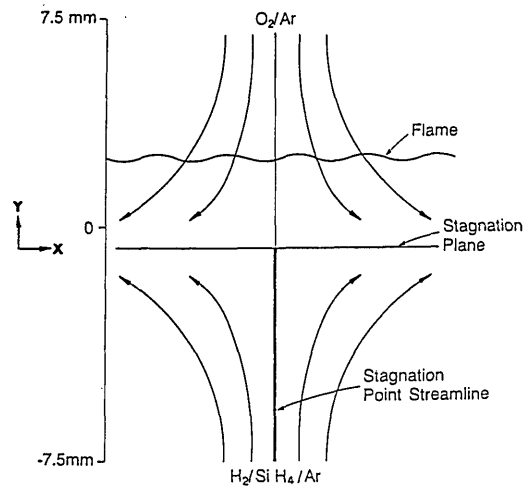

Fig. 3. Schematic of counterflow diffusion flame flow field. (The dark line, corresponding to the stagnation point streamline, marks the region probed by the laser.)

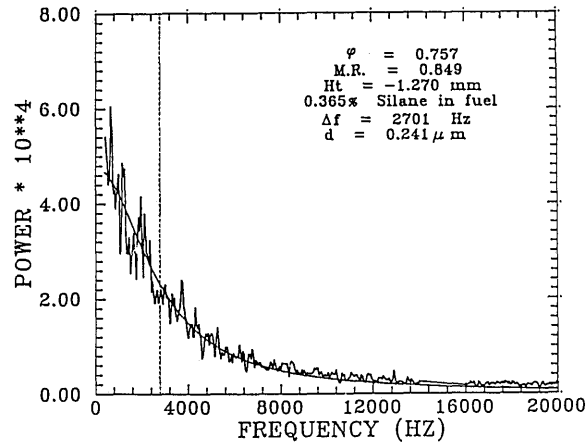

Fig. 4. Example of a dynamic light scattering power spectrum and an associated Lorentzian fit.

tensive discussion of the reactor characteristics can be found elsewhere.[16] Silane (SiH_4) is used as the source of silicon, and the formation of silica follows the overall reaction

$$SiH_4 + 2O_2 = SiO_2 + 2H_2O$$

in the presence of a hydrogen–oxygen flame. All measurements were conducted along the stagnation point streamline by traversing the reactor vertically with a stepping motor.

V. Results and Discussion

We have varied a number of process parameters (temperature, H_2–O_2 ratio, silane loading, and flow velocity) in an effort to observe changes in particle growth regimes and final particle morphology.[12] For the purposes of this paper, some of the results from three flames are presented. A relatively cool flame with peak temperatures of 2000 K is shown, and two hotter flames (peak temperature ≈ 2500 K) are presented.

Figure 4 is an example of the power spectrum obtained from a DLS experiment along with the associat-

ed Lorentzian fit (solid curve). The vertical dotted line corresponds to the frequency at half-maximum, from which the particle size is calculated. Figure 5 presents a comparison of particle diameter measurements obtained using the DLS and LSD techniques. In addition, the calibrated scattering intensity Q_{vv} (45°) is plotted for comparison. It is clear that in some regions of the flame the agreement is quite good, while in other regions we find considerable disparity between the two techniques. It is worthwhile to consider some other comparisons before embarking on a discussion of the reasons for the discrepancy. Figures 6 and 7 are profiles for two additional flames which are at a higher temperature ($T > 2500$ K).

In all three flames, agreement between the two techniques is extremely good in the central portion of the particle field. Near the entrance to the reactor and toward the center, however, there is a marked divergence in the diameters obtained. In all cases the dissymmetry measurement, where it diverged from DLS, always indicated larger particles. It is also clear that in those regions where particle scattering intensity was greatest, agreement between the two techniques was best. As the scattering intensity declined toward both the entrance and exit regions of the reactor, the two techniques diverged.

To understand these discrepancies and infer which if any of the profiles is more nearly correct, it is necessary to consider some of the factors affecting the results. The diffusion coefficient of a particle is highly temperature dependent (for free molecular flow $D \alpha T^{3/2}$) and in flame conditions can be considerably larger than those of ambient aerosols. Recalling Eq. (3), we see that the measured halfwidth is directly proportional to the diffusion coefficient, which under flame temperatures can be extremely large. This necessitates the use of small scattering angles ($\theta < 10°$) to avoid overflowing the frequency range of the spectrum analyzer (100 kHz). Small particles, or alternately particles with high diffusion coefficients (due to high temperatures), will effectively spread the scattering signal over a wider range of frequency space, lowering signal to noise, and thereby enhancing the shot noise contribution to the power spectrum, which is frequency independent. This results in a broader power spectrum which translates into an artificially large diffusion coefficient and, therefore, smaller particle size. At small scattering angles, decreasing the scattering angle by a factor of 2, can affect a fourfold decrease in the halfwidth [see Eq. (2)]. This, however, results in a decreased spatial resolution, which necessitates stopping down on the apertures to define an equivalent scattering volume, and coherence area, resulting in a lower signal at the detector. The lower signal intensity manifests itself as a contribution of the shot noise term and lower SNR. It can be shown that to obtain a halfwidth accuracy of 10%, a SNR of the order of 100 is required. In some conditions we were unable to obtain SNRs of better than 5. These generally occurred in those regions where the scattering intensity was low, either near the entrance of the reactor or near the stagnation plane, as seen in the previous figures.

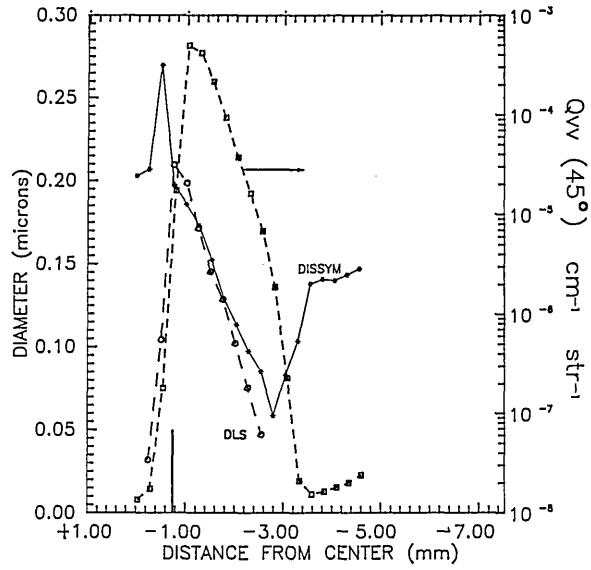

Fig. 5. Axial profiles of DLS and dissymmetry particle diameters and corresponding $Q_{vv}(45)$ scattering cross sections. Verticle bar corresponds to experimental particle stagnation points. H_2–O_2 ratio = 1.51, $X_{Ar} = 0.67$, $T_{peak} = 1990$ K, X_{SiH4} in fuel = 0.21 mole%, fuel velocity = 6.6 cm/s, oxidizer velocity = 5.4 cm/s.

Dissymmetry measurements, or any other elastic light scattering, need not work at such shallow angles and are not constrained by the coherence limitations, which decrease the amount of light collected. Furthermore, since the total scattering intensity (without frequency discrimination) is measured, these techniques provide significantly higher SNR and, therefore, more reliable measurements at lower scattering intensities.

The dissymmetry diameter profiles exhibit some interesting features, which may be thought to encompass three distinct regions. The verticle bar marks the location of the apparent (particle size dependent) stagnation point. The location of the stagnation point seems to be a function of the particle size and magnitude of the thermophoretic force acting in opposition to the convective flow. Downstream of the apparent stagnation point, an abrupt jump in particle size is observed, arising from the large particles (small in number) with associated smaller thermophoretic force penetrating closer to the gas stagnation point, with the bulk of silica having been ejected from the burner. The region near the reactor entrance exhibits unusually large particles which are again small in number and probably arise from reintrainment of particles subsequent to deposition on the burner face. The decrease in particle size near the stagnation point of the two hotter flames (Figs. 6 and 7) results from sintering of the agglomerate as well as dislodging of some of the loosely attached primary particles, as evidenced from the increase in number density near the stagnation point (Fig. 8). Corroboration of this effect is seen in electron micrographs of samples taken from this region. A more thorough discussion of the results may be found in Ref. 16.

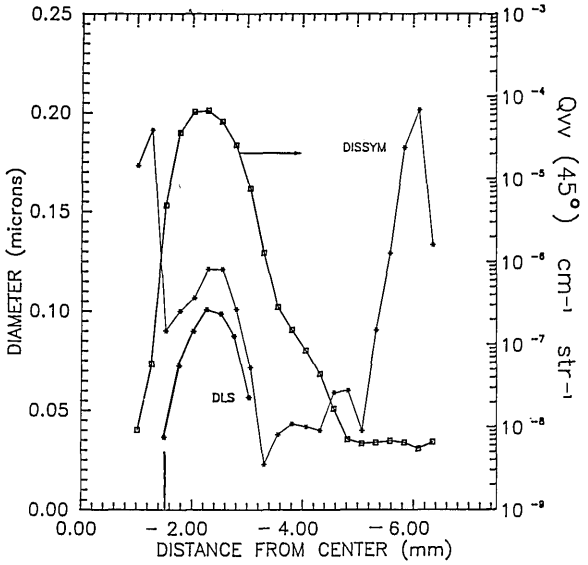

Fig. 6. Axial profiles of DLS and dissymmetry particle diameters and corresponding $Q_{vv}(45)$ scattering cross sections. High temperature flame. Verticle bar corresponds to experimental particle stagnation points. H_2–O_2 ratio = 1.36 X_{Ar} = 0.41, T_{peak} = 2530 K, X_{SiH4} in fuel = 0.356 mole, fuel velocity = 12.2 cm/s, oxidizer velocity = 9.8 cm/s.

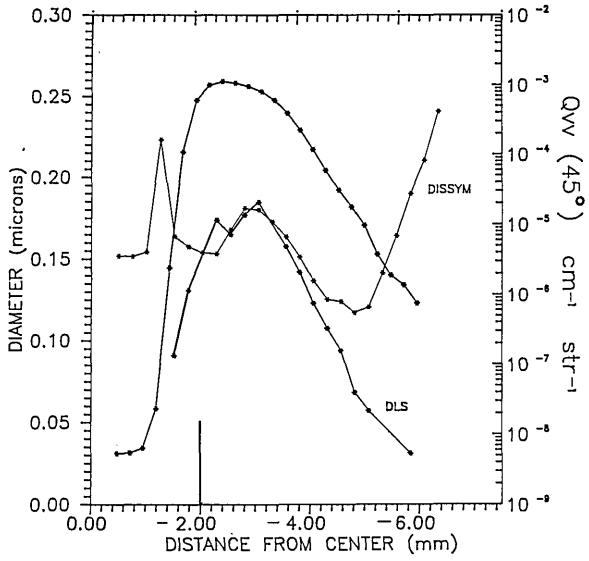

Fig. 7. Axial profiles of DLS and dissymmetry particle diameters and corresponding $Q_{vv}(45)$ scattering cross sections. High temperature flame. Verticle bar corresponds to experimental particle stagnation points. H_2–O_2 ratio = 1.37, X_{Ar} = 0.40, T_{peak} = 2530 K, X_{SiH4} in fuel = 0.20 mole%, fuel velocity = 6.8 cm/s, oxidizer velocity = 5.6 cm/s.

Figure 8 shows the number density and volume fraction profiles based on determination of particle diameter from dissymmetry measurements and the calibrated scattering intensity at $\theta = 45°$. Similar profiles can be generated from the scattering cross section calculated from the DLS measurement when used in conjunction with a single angle scattering experiment. The profiles show the specific regions of nucleation, surface growth, and subsequent expulsion from the reactor as particles reach the stagnation plane. The number density profile suggests that particle nucleation occurs extremely rapidly as evidenced by the abrupt rise in number density followed by a region where particle concentration stays essentially constant. The slight increase in particle number density seen near the stagnation point is evidence of breakup in the agglomerates. The volume fraction curve by comparison shows that in conditions of constant number density, particle growth effects are extremely significant and indeed show that the majority of particle mass at the stagnation point was a result of surface growth processes.

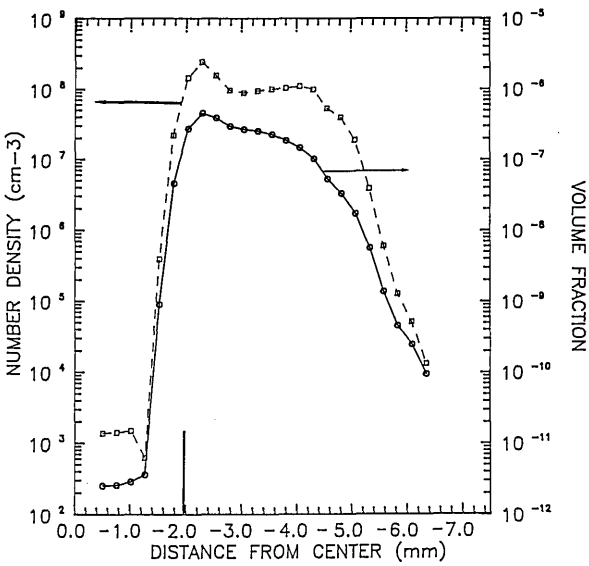

Fig. 8. Axial profiles of number density and volume fraction corresponding to dissymmetry measurements of Fig. 7. Verticle bar corresponds to experimental particle stagnation points.

VI. Conclusions and Recommendations

It is important to summarize what has been learned by the comparison between DLS and dissymmetry and detail the general efficacy of a particular technique for a given set of circumstances. We have seen that in conditions of high SNR both techniques compare very favorably. In fact it is quite surprising that the two techniques, which rely on completely different physical principles for particle sizing, should compare at all when one considers that the underlying theory applied implicitly assumes that the particles are spherical and monodisperse, which is clearly not the case for particles generated in this manner. What it suggests is that for smaller aggregates the hydrodynamic radius (measured by DLS) and the Mie scattering volume (measured by LSD) are very nearly equivalent. This would not be the case were we able to make the same measurements on single particles; however, by making an ensemble measurement we obtain orientation and shape averaged spherical scattering and hydrodynamic volumes. It is possible that for larger aggregates this would not be the case and a fractal analysis approach would be more appropriate.[17]

In terms of general applicability to a chosen problem, we have tabulated (Table I) those points which

Table I. Elastic vs Dynamic Light Scattering

	Elastic	Dynamic
Particle size	$d/\lambda > 0.1$ for dissymmetry, two-color, polarization ratio techniques. No size limitations for scattering/extinction.	No size limit in principle. However, poor sensitivity for small particles.
Temperature	Temperature dependence on refractive index, usually weak.	$Kn > 10$ $Kn < 10$
		$D\alpha T^{3/2}$ $D\alpha T^{1/2}$
		$d\alpha T^{-3/4}$ $d\alpha T^{-1/2}$
Gas composition	Generally unimportant	$d\alpha MW^{1/4}$ $d\alpha MW^{1/2}$
Flow velocity	Unimportant	Corrections may be necessary (see text)
Spatial resolution	Good resolution	Small scattering angles. Poor resolution.
	(In general in flame conditions spatial resolution of DLS not as good as elastic)	
Particle shape	Measures scattering area. Important effects for large agglomerates of >100 primary particles.	Measures hydrodynamic radius. Shape effects on drag for large agglomerates may be important.
Polydispersity	Heavily weighted toward larger particles scattering intensity αd^6 in Rayleigh limit.	

should be addressed prior to choosing a diagnostic technique. DLS has the advantage that particle sizing can be made without knowledge of refractive index, which is important when the exact compositional nature of the particles is unknown. However, as we have seen the measurement does not possess the sensitivity of a classical technique. Additionally, some knowledge of the temperature field and gas composition is required, neither of which may be easily obtained in a highly reactive nonisothermal flow. Indeed one needs a good description of the flow field to classify Doppler broadening effects. Finally DLS cannot, certainly when working in high temperature or small particle environments, match the spatial resolution of an elastic light scattering measurement.

References

1. G. D. Ulrich, "Flame Synthesis of Fine Particles," Chem. Eng. News 22 (6 Aug. 1984).
2. R. A. Dobbins, R. J. Santoro, and H. G. Semerjian, "Interpretation of Optical Measurements of Soot in Flames," Prog. Astronaut. Aeronaut. **92,** 208 (1983).
3. A. D'Allesio, "Laser Light Scattering and Fluorescence Diagnostics of Rich Flames Produced by Gaseous and Liquid Fuels," in *Particulate Carbon-Formation During Combustion*, D. C. Siegla and G. W. Smith, Eds. (Plenum, New York, 1981), p. 207.
4. W. Hinds and P. C. Reist, "Aerosol Measurement by Laser Doppler Spectroscopy-II, Operational Limits, Effects of Polydispersity, and Applications," Aerosol Sci. **3,** 501 (1972).
5. G. B. King, C. M. Sorenson, T. W. Lester, and J. F. Merklin, "Direct Measurement of Aerosol Diffusion Constants in the Intermediate Kundsen Regime," Phys. Rev. Lett. **50,** 1125 (1983).
6. W. L. Flower, "Measurements of Diffusion Coefficients for Soot Particles," Phys. Rev. Lett. **51,** 2287 (1983).
7. J. F. Driscoll, D. M. Mann, and W. K. McGregor, "Submicron Particle Size Measurements in an Acetylene–Oxygen Flame," Combust. Sci. Technol. **20,** 41 (1979).
8. W. L. Flower, "Optical Measurement of Soot Formation in Premixed Flames," Combust. Sci. Technol. **33,** 17 (1983).
9. B. Chu, *Laser Light Scattering* (Academic, New York, 1974).
10. R. Pecora, *Dynamic Light Scattering* (Plenum, New York, 1985).
11. H. Z. Cummins and H. L. Swinney, "Light Beating Spectroscopy," Prog. Opt. **8,** 135 (1970).
12. G. M. Hidy and J. R. Brock, *The Dynamics of Aerocolloidal Systems* (Pergamon, Oxford, 1970).
13. S. F. Friedlander, *Smoke Dust and Haze* (Wiley, New York, 1977).
14. C. N. Davies, "Definative Equation for the Fluid Resistance of Spheres," Proc. R. Soc. London **57,** 259 (1945).
15. J. V. Dave, "Subroutines for Computing the Parameters of the Electromagnetic Radiation Scattered by a Sphere," IBM Scientific Center Report 320-3237 (1968).
16. M. R. Zachariah, D. Chin, H. G. Semerjian, and J. L. Katz, "Silica Particle Synthesis in a Counter Flow Diffusion Flame Reactor," to be published in Combust. Flame.
17. A. J. Hurd and W. L. Flower, "In Situ Growth and Structure of Fractal Silica Aggregates in a Flame," to be published in J. Colloid Interface Sci.